Mutation of mouse *Mayp/Pstpip2* causes a macrophage autoinflammatory disease

Johannes Grosse, Violeta Chitu, Andreas Marquardt, Petra Hanke, Carolin Schmittwolf, Lutz Zeitlmann, Patricia Schropp, Bettina Barth, Philipp Yu, Rainer Paffenholz, Gabriele Stumm, Michael Nehls, and E. Richard Stanley

Macrophage actin–associated tyrosine phosphorylated protein (MAYP)/PSTPIP2, a PCH protein, is involved in the regulation of macrophage motility. Mutations in a closely related gene, *PSTPIP1/CD2BP1*, cause a dominantly inherited autoinflammatory disorder known as PAPA syndrome. A mutant mouse obtained by chemical mutagenesis exhibited an autoinflammatory disorder characterized by macrophage infiltration and inflammation, leading to osteolysis and necrosis in paws and necrosis of ears. Positional cloning of this recessive mutation, termed *Lupo*, identified a T to A nucleotide exchange leading to an amino acid substitution (I282N) in the sequence of MAYP. *Mayp*$^{Lp/Lp}$ disease was transferable by bone marrow transplantation and developed in the absence of lymphocytes. Consistent with the involvement of macrophages, lesion development could be prevented by the administration of clodronate liposomes. MAYP is expressed in monocytes/macrophages and in a Mac1^{+} subfraction of granulocytes. LPS stimulation increases its expression in macrophages. Because of the instability of the mutant protein, MAYP expression is reduced 3-fold in *Mayp*$^{Lp/Lp}$ macrophages and, on LPS stimulation, does not rise above the level of unstimulated wild-type (WT) cells. *Mayp*$^{Lp/Lp}$ mice expressed elevated circulating levels of several cytokines, including MCP-1; their macrophages exhibited altered cytokine production in vitro. These studies suggest that MAYP plays an anti-inflammatory role in macrophages. (Blood. 2006;107:3350-3358)

Introduction

Autoinflammatory diseases are systemic conditions involving apparently unprovoked inflammation in the absence of autoantibody- and antigenic-specific T cells. A significant proportion of these diseases is caused by single gene mutations. Furthermore, the mutated gene remains to be discovered in a number of Mendelian inherited autoinflammatory diseases.[1] Identifying the genes involved is a first step toward elucidating the pathways involved in the inflammatory processes underlying these diseases. Among the genes recently identified as causal is the gene encoding the TNF receptor, which has long been recognized for its role in inflammation and immunity. TNF receptor–associated periodic syndrome (TRAPS) is caused by mutations in the extracellular domain of the 55-kDa TNF receptor that lead to a dominantly inherited periodic fever.[2] Leukocytes from some, but not all, of these patients have increased membrane TNFRS1A and impaired receptor ectodomain cleavage on in vitro stimulation, consistent with a deficiency in a normal negative homeostatic process.[3]

Two autoinflammatory periodic fever syndromes in which the mutated gene has been identified recently point to a common pathway.[4] Familial Mediterranean fever (FMF) is an autosomal recessive disorder resulting from mutations in the gene encoding pyrin, which normally inhibits pro–IL-1β cytokine processing to the active form. It has recently been shown that mutations in the structural gene encoding Pombe Cdc15 homology (PCH) family protein, proline serine threonine phosphatase-interacting protein 1/CD2 binding protein 1 (PSTPIP1/CD2BP1),[5] lead to an autosomal-dominant autoinflammatory disease called pyogenic arthritis, pyoderma gangrenosum, and acne (PAPA) syndrome.[6] These mutations lead to decreased binding of PSTPIP1 to a protein tyrosine phosphatase, PTP-PEST, that specifically dephosphorylates PSTPIP1.[6,7] Subsequent studies by Shoham et al[8] showed that pyrin, the protein involved in FMF, interacts with PSTPIP1, thus establishing an important biochemical link between the proteins involved in these 2 diseases. Clearly, identification of the genes mutated in autoinflammatory diseases such as TRAPS, FMF, and PAPA, coupled with increased understanding of the functions of the proteins encoded by them, promises to greatly increase our knowledge of the mechanisms that mediate leukocyte inflammatory responses.

PCH proteins constitute an extensive protein family involved in the regulation of actin polymerization and actin-based processes, including membrane ruffling, formation of filopodia, cell adhesion, and cytokinesis.[9-15] The PCH protein, macrophage actin-associated tyrosine phosphorylated protein (MAYP),[11] closely related to PSTPIP1 and also known as PSTPIP2,[12] is expressed in macrophages and macrophage-containing tissues.[11] Like that of PSTPIP1 and the other PCH family members, its domain organization includes an amino-terminal Fes-CIP4 homology (FCH) domain

From Ingenium Pharmaceuticals, Martinsried, Germany; and the Department of Developmental and Molecular Biology, Albert Einstein College of Medicine, Bronx, NY.

Submitted September 2, 2005; accepted November 30, 2005. Prepublished online as *Blood* First Edition Paper, January 5, 2006; DOI 10.1182/blood-2005-09-3556.

Supported by grants from the National Institutes of Health (grant CA25604; E.R.S.), the Albert Einstein College of Medicine Cancer Center (grant 5P30-CA13330), and the European Union (Euro-Thymaide) and by Postdoctoral Fellowship Research Award PDF0201811 from the Susan G. Komen Breast Cancer Foundation (V.C.).

J.G. and V.C. contributed equally to this study.

An Inside *Blood* analysis of this article appears at the front of this issue.

Reprints: E. Richard Stanley, Department of Developmental and Molecular Biology, Albert Einstein College of Medicine, 1300 Morris Park Ave, Bronx, NY 10461; e-mail: rstanley@aecom.yu.edu.

The publication costs of this article were defrayed in part by page charge payment. Therefore, and solely to indicate this fact, this article is hereby marked "advertisement" in accordance with 18 U.S.C. section 1734.

(amino acids 13-98) and a coiled-coil domain (amino acids 93-121). However, MAYP/PSTPIP2 lacks the carboxy-terminal SH3 domain that mediates their interaction with WASP/N-WASP proteins involved in the regulation of actin polymerization.[11,12] In macrophages, MAYP is tyrosine phosphorylated in response to CSF-1, which also stimulates macrophage actin reorganization, membrane ruffling, increased filopodia formation, motility, and chemotaxis.[16] Studies in which MAYP was overexpressed and underexpressed in macrophages indicate that MAYP is a negative regulator of CSF-1–induced membrane ruffling and positively regulates the formation of filopodia and directional migration.[11,15] In this paper, we describe a mouse MAYP mutation that leads to a macrophage-based autoinflammatory disease associated with lowered MAYP expression in macrophages.

Materials and methods

Mice, mutagenesis, positional cloning, and genotyping

C3HeB/FeJ (stock no. 000658), C57BL/6J (stock no. 000664), C57BL/6J Ly5.1 (CD45.1) (stock no. 002014), and C57BL/6J Rag1$^{-/-}$ (stock no. 002216) mice were obtained from the Jackson Laboratory and kept at a 12-hour light/12-hour dark cycle with food and water available ad libitum in full-barrier facilities free of specific pathogens according to the Federation of European Laboratory Animal Science Associations (FELASA).[17] Mouse breeding and all experimental procedures were approved by the responsible governmental authorities. Mutagenesis was performed as described.[18,19] Briefly, male C3HeB/FeJ mice were treated intraperitoneally with *N*-ethyl-*N*-nitrosourea, 3 × 90 mg/kg. Offspring of these males (F1) were bred, and the next generation (F2) was intercrossed to generate mice homozygous for subsets of the introduced mutations (F3). For positional cloning, affected mice were outcrossed to the C57Bl/6J strain, and resultant hybrids were intercrossed. Offspring were tested for the phenotype, and mouse DNA was prepared from tail clips using the DNeasy Tissue Kit (Qiagen, Valencia, CA). Standard polymerase chain reaction (PCR) was performed with 40 ng genomic DNA per reaction. For the initial chromosomal mapping, 45 genomewide-distributed microsatellite markers discriminating between C3HeB/FeJ and C57BL/6J were analyzed on an ABI 3700 (GE Healthcare Life Sciences, Fairfield, CT) device using the Genotyper 3.6 software. Fine mapping was performed by gel electrophoresis analysis of polymorphic microsatellite markers on an ethidium bromide–stained 3.5% agarose gel. Oligonucleotide sequences for PCR analysis of public microsatellite markers were taken from http://www.broad.mit.edu/cgi-bin/mouse/sts_info?database=mouserelease. Oligonucleotide sequences of novel microsatellite markers are as follows: D18Ing123-1, 5′-AGTTCACCTATAAATCTCTAGTAT-3′; D18Ing123-2, 5′-TCAACACACTCAGATTTGACTGA-3′; D18Ing106-1, 5′-TTCATCCAAATGACATTCCAA-3′; D18Ing106-2, 5′-CCCTGGCTAATCTTTATTTGCT-3′; D18Ing112-1, 5′-CAGCATGTCAACAAAGAGCA-3′; D18Ing112-2, 5′-CAGACTGGGGTTCAGAGTGC-3′. PCR amplification and sequencing of the Pstpip2 mutation was performed using oligonucleotide sequences 5′-CCAGCCTCTACATGCTTCTG-3′ and 5′-TCTTACATCATTAATAGCATAGAC-3′. For Pstpip2 mutation genotyping, the primers 5′-GGGAGTGTAGAAAGCCTCCTT-3′ and 5′-TTCCAAGACAGGGTCTCATGT-3′ were used. All oligonucleotide primers were synthesized (MWG Biotech AG, Ebersberg, Germany).

Bone marrow transplantation

Mice of the mixed C3H/BL6 background were genotyped at the H-2 locus. Donors were b/b, and recipients were b/b or k/b. Recipients were irradiated with 9.5 Gy (950 rads) and 2 × 10^6 cells in 200 μL PBS were injected intravenously. Repopulation by donor-derived bone marrow was tested using Ly5.1 as marker by FACS analysis of peripheral blood. A similar procedure was used for the transfer in the C3H inbred background, except that the irradiation dose was 9 Gy (900 rad).

FACScan hematologic and x-ray analyses

Monoclonal antibodies conjugated to fluorescein isothiocyanate (FITC), phycoerythrin (PE), or allophycocyanin (APC) were from Becton Dickinson (Heidelberg, Germany). Cells were analyzed on a FACSCalibur (Becton Dickinson). The following marker panels were used to characterize tissue-derived cell populations: blood—B220, CD45RB, DX5, CD44, Gr-1, CD122, CD4, CD3, CD8b; lymph node—CD45RB, DX5, CD44, CD122, CD4, CD8b, CD25, CD3; spleen—DX5, CD122, CD3, CD8b; thymus—CD45RB, CD44, CD4, CD25; Peyer patches—B220, CD45RB, DX5, CD44, Gr-1, CD122, CD4, CD3, CD8b, CD25, CD25, CD11b; peritoneal lavage—IgD, IgM, B220, CD5, CD43, CD11b. For hematologic analyses, white and red blood cell counts; lymphocyte, monocyte, and granulocyte counts; platelet counts; hemoglobin level; hematocrit; mean red blood cell (RBC) volume; mean platelet volume; mean cellular hemoglobin level; mean cellular hemoglobin concentration; and RBC distribution width were determined using a Veterinary Animal Blood Counter according to the manufacturer's recommendation (Scil Animal Care Company, Viernheim, Germany). Radiographs were generated using a Faxitron Radiography System (model MX-20; Faxitron X-Ray, Wheeling, WV).

Serum immunoglobulins

Mice were starved overnight and bled, and the heparinized plasma was diluted 1:75 in PBS/1% BSA/0.01% NaN_3. Isotype-specific anti–mouse IgG_1, IgG_{2a}, IgG_{2b}, IgG_3, IgA, IgM, and IgE capture antibodies were coupled to different sets of fluorogenic microspheres according to manufacturer's protocols (Luminex, Austin, TX). Mixtures of microspheres (9-fold multiplexed) were incubated with the diluted plasma, and biotin-labeled mouse isotype antibodies were added as competitors. Competitors were detected by measuring streptavidin-PE (PharMingen, San Diego, CA) and microsphere fluorescence on a Luminex-100 analyzer (Luminex).

Analysis of autoantibodies

Paw proteins of wild-type (WT) mice were extracted from powdered frozen-tissue fragments with SDS sample buffer and equivalent amounts of protein per lane, subjected to 12% SDS-PAGE, and transferred to membrane, and separate lanes were individually incubated for 1 hour with different sera (dilution, 1:1000) taken at day 50 from 6 individual WT or 6 *Mayp*$^{Lp/Lp}$ mice. Autoreactive antibodies were detected using an anti–mouse IgG secondary antibody and the enhanced chemiluminescence (ECL) detection procedure (Amersham Bioscience, Freiburg, Germany).

Clodronate treatment

Phosphatidylcholine (LIPOID E PC) was obtained from Lipoid GmbH (Ludwigshafen, Germany), and cholesterol was obtained from Sigma (Deisenhofen, Germany). Clodronate (dichloromethylene bisphosphonate (Cl_2MBP) and control liposomes were prepared as described.[20] Clodronate or PBS (control) liposomes were administered intraperitoneally (200 μL twice weekly) or simultaneously intraperitoneally (200 μL, twice weekly) and subcutaneously into the hind paws (12 μL, once weekly) of 4-week-old *Lupo* mice. Inflammation was monitored every third day.

Histology

Histopathologic examination was performed according to standard procedures and was followed by H&E staining. For immunochemistry (IHC), the feet of WT animals were immersion fixed in 4% formalin in PBS, followed by decalcification using 20% EDTA frequently changed during 2 weeks. Sections were pretreated with 0.1% Pronase E (10 minutes, 20°C; Sigma Aldrich, Poole, United Kingdom) and incubated with *Lupo* serum at a 1:750 dilution. Secondary antibody was biotinylated goat antimouse (1:500; Vector), detected with peroxidase-labeled streptavidin and Novared as chromogen (both from Vector), and counterstained with Mayer hematoxylin (Chroma, Germany). F4/80 staining was performed as described previously.[21]

For light microscopy, Zeiss Axioplan 2 (Figures 2A-B, 4C) and Zeiss AxioSkop 2 (Figure 2C-F) microscopes were used, and imaged using an AxioCam MRc camera and Axiovision 4.1 software (all from Carl Zeiss, Oberkochen, Germany). Plan Neofluar objectives used included 20 ×/0.5

numeric aperture (NA) (Figures 2A-B, 4C), 2.5 ×/0.075 NA (Figure 2C,E), and 25 ×/0.8 NA (Figure 2D,F). Images were cropped and adjusted for brightness and color saturation using Adobe Photoshop Elements 2.0 (Adobe Systems, San Jose, CA).

Blood cell fractionation and immunofluorescence analysis

Human blood was obtained from healthy donors. Peripheral blood mononuclear cells (PBMCs) were separated from granulocytes and red blood cells using Ficoll-Hypaque (Pharmacia, Uppsala, Sweden). Granulocytes were separated using dextran and hypotonic lysis as described,[22] and monocytes were depleted from the PBMC fraction by adherence (2 hours, 37°C). Granulocytes and nonadherent PBMCs (lymphocytes) were then pelleted and lysed with 2% SDS. Adherent PBMCs (monocytes) were rinsed 5 times with PBS and lysed on the plate with 2% SDS. For immunofluorescence and monitoring purification, aliquots of the monocyte and granulocyte fractions were cytocentrifuged onto poly-L-lysine–coated coverslips and fixed with 3.7% paraformaldehyde. Immunofluorescence staining of MAYP was performed as described.[15] For analysis of mouse blood, leukocytes were prepared by hypotonic lysis and FACS-sorted based on the expression of Mac1 and Gr1 antigens, and aliquots were cytocentrifuged, fixed, and stained as described. All samples were examined under an Olympus IX70 inverted microscope (Olympus, Melville, NY) with a 60 ×/1.4 NA oil-immersion objective, and images were recorded using a Photometrics CH cooled charged coupled device (CCD) camera and IP lab spectrum software (VayTek, Fairfield, IA). Images were artificially colored and adjusted for brightness and color saturation using Adobe Photoshop Elements 2.0. MAYP expression was examined by Western blot of SDS cell lysates (10 μg/lane).

Measurement of MAYP and cytokines in BMM

Bone marrow–derived macrophages (BMMs) were prepared and cultured in 120 ng/mL CSF-1 (a gift from Chiron, Emeryville, CA), as described previously.[23,24] For LPS stimulation experiments, BMMs were seeded into the wells of 96-well (10^5 cells/200 μL) or 6-well (10^6 cells/5 mL) culture dishes and were incubated overnight at 37°C, before a medium change (100 μL or 2 mL, respectively) to serum-free α-MEM (Gibco, Grand Island, NY) containing CSF-1, supplemented with 100 μg/mL endotoxin-free BSA with or without LPS (1 μg/mL) for specified times. Supernatants were removed and stored at −80°C. Cells were rinsed with PBS, lysed with 2% SDS, and analyzed by SDS-PAGE and Western blot for protein expression. Supernatant cytokines were measured by incubating supernatants (1.5 mL) with a mouse inflammation array (Ray Biotech, Norcross, GA) consisting of 40 cytokine and chemokine antibodies spotted in duplicate onto a membrane, according to the instructions of the manufacturer. Supernatants were obtained from 6-well overnight cultures of equivalent cell numbers of WT and *Mayp*$^{Lp/Lp}$ BMMs. To confirm the equivalence of the cell numbers, 50-μL aliquots of the cell lysates were subjected to SDS-PAGE and Western blotting with β-actin. Chemiluminescence was measured in a Fujifilm LAS3000 imager (Fuji, Tokyo, Japan) and quantified using MultiGauge software (Fuji) from the manufacturer. For each spot, the net density gray level was determined by subtracting the background gray levels from the total raw density gray levels. The relative fold difference in cytokine amount in *Mayp*$^{Lp/Lp}$ BMM supernatants was determined with reference to the amount present from the WT culture on the same membrane. Antibodies to the following cytokines were arrayed: BLC, CD30L, Ltaxin, Eotaxin-2, Fas ligand, Fractalkine, G-CSF, GM-CSF, IFN-γ, IL-1α, IL-1β, IL-2, IL-3, IL-4, IL-6, IL-9, IL-10, IL-12p40p70, IL-12p70, IL-13, IL-17, I-TAC, KC, Leptin, LIX, Lymphotactin, MCP-1, M-CSF, MIG, MIP-1α, MIP-1γ, RANTES, SDF-1, TCA-3, TECK, TIMP-1, TIMP-2, TNF-α, sTNFRI, and sTNFRII. Western blots and immunoprecipitations using a purified rabbit anti–MAYP peptide antibody were carried out with equal amounts of cell lysate protein, as described previously.[15]

Quantitative RT-PCR

BMMs were plated in 6-well culture dishes and stimulated with LPS as described. Total RNA was isolated using the RNeasy kit (Qiagen) and stored at −80°C until use. cDNA was obtained by reverse transcription from 2.5 μg total RNA using the SuperScriptIII One-Step RT-PCR System (Invitrogen, Carlsbad, CA). Real-time PCR was performed with triplicate samples using the SYBR Green PCR Kit (Qiagen) and primers for MAYP (5′ TGCAGCATTGAGAAGGACATC, 3′ CATTCCGCTGAGGAGAGTAGAAG) and beta-actin.

Results

Identification of mutant mouse and description of gross inflammatory phenotype

The progeny of mice bearing genomewide random mutations were bred to generate animals homozygous for subsets of the introduced mutations. Phenotypic screening for abnormalities by visual inspection, neurologic and behavioral tests, and clinical chemistry and hematology parameters identified a mouse with edematous swollen and inflamed toes. Further breeding revealed a recessive inheritance of the trait, and the line was named *Lupo*. The first clinical signs are usually edematous or bullous inflammation of individual toes (Figure 1A), progressing to involve further toes and palmar or plantar regions of the same and other extremities. Inflamed areas are erythematous, scaly, or ulcerated; they often ooze and have subsequent crust formation. In advanced stages, adjacent toes adhere together and osteolysis sets in, resulting in localized necrosis of toes within an extremity (Figure 1B, D). The ears are

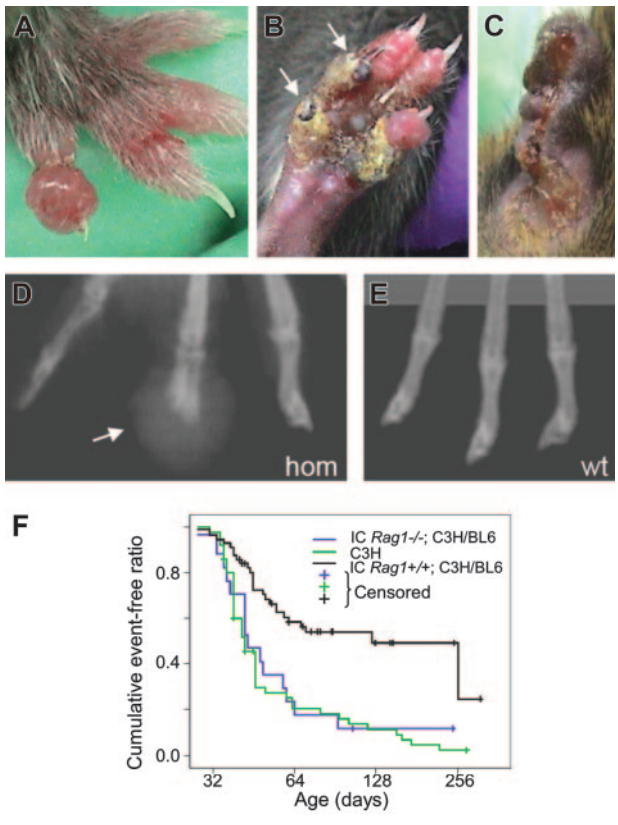

Figure 1. Clinical symptoms and disease progression in homozygous *Lupo* mice. (A-B) Early clinical symptoms with edematous inflammation, proceeding to ulceration, crust formation, and necrosis of 2 digits (B, arrows). (C) Ear destruction by ulcerative inflammation. (D) Radiogram showing the destruction of the distal phalanx of digit 3 in a homozygous mutant mouse. Note the shadow caused by the surrounding edematous soft tissue (arrow). (E) Radiogram of WT control paw. (F) Cumulative fraction free of clinical events for *Lupo* homozygotes on the C3H background, in outcross/intercross (IC) *Rag1*$^{+/+}$, C3H/BL6 (50%/50%) population used for positional cloning and on the *Rag1*$^{-/-}$, C3H/BL6 (50%/50%) background. On the *Rag1*$^{+/+}$, C3H/BL6 background, the median age of onset was significantly later, and lifetime penetrance was lower than on the C3H or the *Rag1*$^{-/-}$, C3H/BL6 background (Kaplan-Meier with log rank test [$P < .001$] for C3H/BL6 versus C3H and C3H/BL6 versus *Rag1*$^{-/-}$, C3H/BL6; censored, termination of observation without an event).

also affected by ulcerative inflammation resulting in necrotic destruction (Figure 1C), but involvement of additional areas was not observed, and overall survival was not affected. In the C3H inbred background, the phenotype is completely penetrant. First clinical signs are usually observed at 6 weeks of age (Table 1; Figure 1F).

Histology of paws and dermis

Histologic analysis revealed an infiltration of the dermal connective tissue in early stages that eventually affected all layers of the skin (Figure 2A). The morphology of the infiltrating cells revealed the presence of some polymorphonuclear cells, plasma cells, and small lymphocytes among other, less clearly defined cells. In advanced stages, interphalangeal articulations and phalangeal bones were eroded (Figure 2B), reflecting osteolysis. Staining with antibody to the tissue macrophage marker, F4/80, revealed extensive infiltration of the interphalangeal regions of the paws by macrophages (Figure 2E-F). In addition, the increased thickening of the dermis in sections of the ear (Figure 2C) was associated with the infiltration of macrophages (Figure 2D). In contrast, granulocytes do not accumulate significantly in early lesions.

Positional cloning

To identify the mutation responsible for disease, affected mice were outcrossed to C57BL/6J (BL6) mice and the offspring intercrossed. Penetrance of the phenotype in this mixed C3H/BL6 background was reduced to 52% (Table 1). Therefore, only affected animals were used for the initial chromosomal mapping through analysis of the allele frequency of 45 polymorphic microsatellite markers distributed genomewide. The phenotype cosegregated with homozygosity for the C3H variant of D18Mit47. To confirm and refine the candidate region, 247 mice originating from the mapping cross-described, and from the cross-breeding with C57BL/6J Rag1$^{-/-}$ (Figure 1F), were analyzed for informative meiotic recombinations using known and novel markers. The critical region was narrowed down to a genomic interval of approximately 2 Mbp flanked by D18Mit106 and D18Ing123 (Figure 3). This interval was inspected for the presence of genes using the mouse genome at http://genome.ucsc.edu. To date, 6 annotated and 2 predicted genes have been mapped to this region. DNA sequence analysis of Pstpip2 (proline-serine-threonine phosphatase-interacting protein 2),[12] synonymous with Mayp,[11] revealed a nucleotide exchange, T to A, in exon 12 at position +845 of RefSeq NM_013831, resulting in an amino acid substitution of isoleucine 282 to asparagine (I282N). This allele is referred to as *Mayp*^{Lp}; consequently, homozygous mice are referred to as *Mayp*$^{Lp/Lp}$. Given the mutation load of our mutagenesis regimen of 1 mutation per 2.69 Mbp,[18] a mapping region of 2 Mbp (9.3% coding sequences), and assuming a constant mutation rate across the genome, the Poisson distributed probability of an unidentified passenger mutation physically linked to *Mayp*^{Lp} was determined to be 0.000016. We concluded that the *Mayp*^{Lp} mutation causes the phenotype.

Table 1. Penetrance and mean age of onset of clinical symptoms in homozygous *Lupo* mutant mice on C3HeB/FeJ (C3H), C3HeB/FeJ × C57BL/6J (C3H/BL6), and C3H/BL6; *Rag1*$^{-/-}$ backgrounds

Parameter	C3H	C3H/BL6	C3H/BL6; *Rag1*$^{-/-}$
Lupo homozygotes, no.	51	57	17
Median age of onset, d	42 ± 4*	124 ± 92*	43 ± 9*
Penetrance, %	98	52	88

Penetrance was scored at 65 days or more and was tested by χ^2 analysis and Fisher exact test. $P < .01$ for C3H/BL6 compared with C3H and for C3H/BL6 compared with C3H/BL6 *Rag1*$^{-/-}$ mice.

*95% confidence limits (CIs).

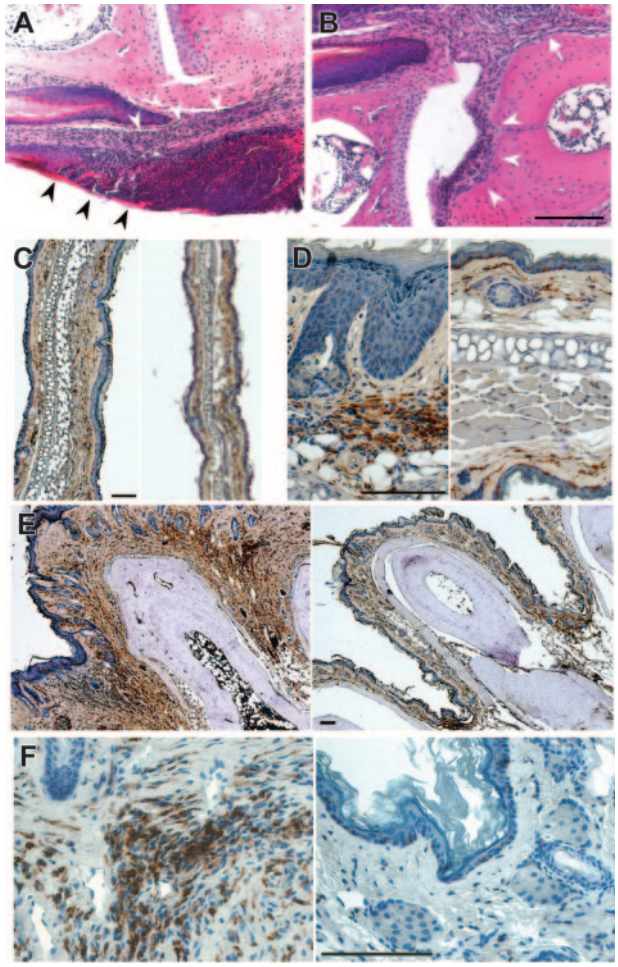

Figure 2. Histology of dermis and paws of homozygous *Lupo* mice. (A-B) Hematoxylin and eosin staining of an early stage of dermal inflammation. Inflammatory infiltration is restricted to the connective tissue of the corium and the epithelium (arrowheads, A) and paws (B), showing inflammation starting from the corium (arrow) and spreading to erode the articular cartilage (arrowheads). (C-D) Low-power (C) and high-power (D) images of ears of *Lupo* (left panels) and WT (right panels) mice, immunostained for the macrophage marker, F4/80+, and counterstained with hematoxylin, showing increased ear thickness, hyperkeratosis, acanthotic epidermis, and increased macrophage infiltration in the external ears of the *Lupo* mice. (E-F) Low-power (E) and high-power (F) images of paws of *Lupo* (left panels) and WT (right panels) mice, immunostained for the macrophage marker F4/80+ and counterstained with hematoxylin, showing increased paw thickness, acanthotic epidermis, and increased macrophage infiltration in the footpads of the *Lupo* mice. Bars, 100 μm.

Hematologic and immunologic parameters of disease

In FACScan analyses with hematologic and lymphoid markers, there was no difference between mutant and WT mice regarding granulocyte, lymphocyte, monocyte, eosinophil, or platelet numbers in peripheral blood or lymphocyte populations isolated from peripheral lymph nodes, spleen, thymus, Peyer patches, or peritoneal lavage and no alteration of the frequency of apoptotic thymocytes (data not shown). In contrast, serum IgG_1, IgG_{2a}, and IgE levels were found to be significantly elevated (Figure 4A). To test for the possibility of antibody-mediated autoimmune disease, we tested the reactivity of *Mayp*$^{Lp/Lp}$ serum against proteins extracted from WT paws. Consistent with the presence of autoantibodies, *Mayp*$^{Lp/Lp}$ mouse serum generated more intense signals and recognized more protein bands than WT serum (Figure 4B). To identify the tissue distribution of these proteins, we performed

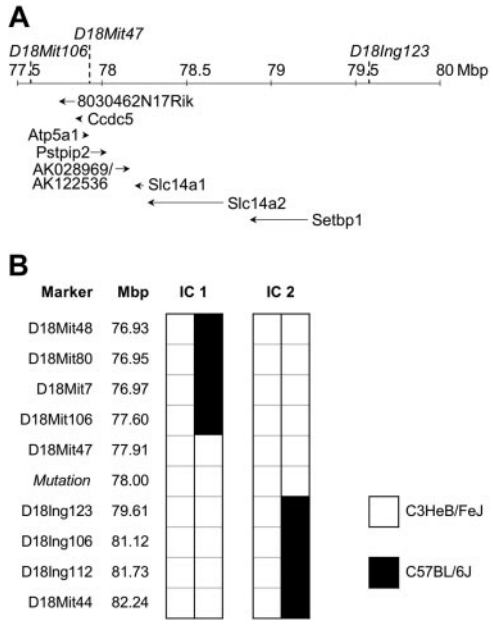

Figure 3. Mapping of the *Lupo mutation.* (A) Genomic structure of the mapping region on chromosome 18. Locations of flanking and cosegregating markers are indicated above the chromosomal ruler and the genes below it. Positions of genes *Ccdc5, Atp5a1, Slc14a1, Slc14a2, Setbp1,* and *Pstpip2/Mayp* and the mapped EST clones 8030462N17Rik and AK028969/AK122536 are shown. (B) Haplotypes of the informative mice (IC1 and IC2) define the mapping region.

immunohistochemical analysis using serum as primary antibody. Most immune reactivity was detected in the papillary layers of the corium, where the inflammation starts to develop (Figure 4C).

Lymphocytes are not required for *Mayp*$^{Lp/Lp}$ disease pathogenesis

To investigate whether autoantibodies and lymphocyte activation are necessary for pathogenesis or are merely inflammation associated, we introduced the *Lupo* mutation onto the lymphocyte-deficient Rag1$^{-/-}$[25] background. *Mayp*$^{Lp/Lp}$ animals (inbred C3H) were crossed with C57BL/6J Rag1$^{-/-}$ mice, and the offspring were intercrossed. As observed in *Mayp*$^{Lp/Lp}$ mice, paw inflammation also developed in the double-homozygous *Mayp*$^{Lp/Lp}$/*Rag1*$^{-/-}$ mice, indicating that lymphocytes are not causally involved in pathogenesis. However, compared with *Mayp*$^{Lp/Lp}$/*Rag1*$^{+/+}$ mice, the double mutant *Mayp*$^{Lp/L}$/*Rag1*$^{-/-}$ mice exhibited an increase in penetrance and an associated decrease in the age of onset (Figure 2; Table 1). Thus, these data indicate that on the mixed C3H/Bl6 background, lymphocytes, instead of exacerbating disease, protect against paw inflammation.

Disease is caused by cells of bone marrow origin

To determine whether the inflammatory disease was of bone marrow origin, bone marrow from the C3H/BL6 mice was transplanted into WT BL6 mice bearing the Ly5.1 allele to distinguish between donor and host repopulations. Repopulation by donor bone marrow was observed in all recipients at 4 and 15 weeks after transfer. One of 5 mice that received transplanted *Mayp*$^{Lp/Lp}$ bone marrow had inflamed paws 4 months after the transfer, but no paw inflammation developed in 5 mice repopulated with WT bone marrow, indicating that the phenotype is transferable by transplantation. That the reduced penetrance of the phenotype resulted from the transplantation of bone marrow from C3H/BL6 mice, with a reduced penetrance phenotype (Figure 1F), was shown by repeat of the adoptive transfer in the more susceptible C3H inbred background. In this case, all 4 WT mice that underwent repopulation with *Mayp*$^{Lp/Lp}$ bone marrow developed the inflammatory phenotype; the first clinical manifestation occurred 6 to 11 weeks after transplantation. Inflammation was progressive, at a rate similar to the rate in C3H-*Mayp*$^{Lp/Lp}$ mice (Figure 1F), and by 17 weeks after transplantation at least 2 paws and both ears in each mouse were affected. Clinical findings and histopathologic appearance were indistinguishable from those of C3H-*Mayp*$^{Lp/Lp}$ mice, and no inflammation occurred in the control group receiving WT bone marrow. This prompted us to question whether the *Lupo* phenotype could be ameliorated by the transplantation of WT bone marrow. Four *Lupo* animals of the mixed C3H/BL6 background that experienced continuous disease for more than 6 months were engrafted with Ly5.1-positive WT C57BL6 bone marrow. During the following 8 weeks, swelling in areas affected before transplantation was greatly reduced and reddening was absent. Oozing areas reepithelialized, and paws were pale in the areas most severely affected before transplantation, suggestive of scar formation. Thus, circulating cells of a nonlymphoid hematopoietic lineage are necessary and sufficient for the development of the inflammation. Furthermore, even after inflammation of long duration, the presence of these cells is required for the maintenance of inflammation.

MAYP is expressed in monocytes/macrophages and Mac1$^+$ granulocytes

Previous studies have reported ubiquitous tissue expression of MAYP mRNA by Northern blot analysis,[12] though Western blot

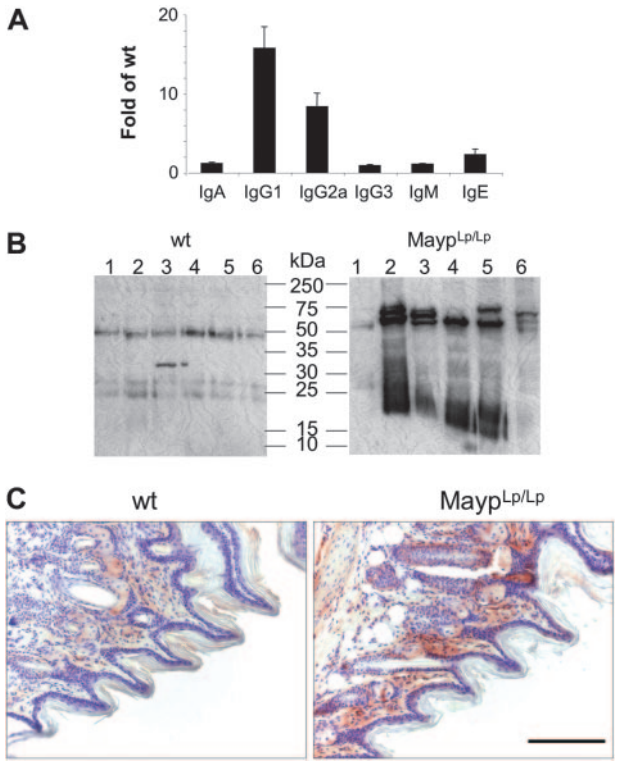

Figure 4. Elevation of circulating immunoglobulin and autoantibodies in 4-month-old *Mayp*$^{Lp/Lp}$ mice. (A) Serum immunoglobulin levels expressed as the fold increase of their concentration in *Mayp*$^{Lp/Lp}$ (n = 5) compared with WT (n = 17) mice (± SD). Elevations of IgG1, IgG2a, and IgE are significant ($P < .05$; Student *t* test). (B) Twelve lanes, each containing identical amounts of a single extract of normal paw proteins, were subjected to SDS-PAGE and Western blot analysis with individual sera of 6 *Mayp*$^{Lp/Lp}$ mice expressing serum immunoglobulin and of 6 WT mice. (C) Immunohistochemistry using serum from a *Mayp*$^{Lp/Lp}$ mouse as primary antibody, showing that the cognate proteins are located in the papillary layers of the corium. Similar results were obtained for 3 additional *Mayp*$^{Lp/Lp}$ sera. Bar, 100 μm.

analysis revealed more restricted expression to tissues expressing high levels of macrophages and in macrophage cell lines.[11] Given that inflammation in the *Mayp*$^{Lp/Lp}$ mice is mediated by cells of a nonlymphoid hematopoietic lineage, we examined the expression pattern of MAYP in white blood cells from mice and humans by anti-MAYP immunofluorescence and Western blot analysis of purified cells. Antibody staining revealed characteristic punctate MAYP cytosolic staining in the Mac1^{hi}Gr1^{lo} monocytes (Figure 5A) and Mac1^{hi}Gr1^{hi} cells with ring-shaped nuclei, previously described as CSF-1R–expressing monocytes or monocyte precursors[26,27] (Figure 5C). Western blot analysis of the Mac1^{hi}Gr1^{hi} cells confirmed their expression of MAYP (Figure 5E). In contrast, diffuse uniform MAYP staining was observed in Mac1^{lo}Gr1^{hi} granulocytes (Figure 5B), and MAYP could not be detected in the granulocyte fraction purified by Ficoll-Hypaque (Figure 5E, Gr) in which a strongly cross-reacting protein of approximately 90 kDa was detected. Mac1^{lo}Gr1^{lo} lymphocytes exhibited slight nuclear staining, reminiscent of a cross-reaction we have previously published for this antibody against a nucleolar protein of approximately 60 kDa[15] (Figure 5E, BMM). A similar expression pattern was reflected in a Western blot analysis of purified lymphocyte, monocyte, and granulocyte fractions from human blood (Figure 5F). Low levels of expression were found in the lymphocyte fraction. Immunofluorescence studies of the lymphocyte fraction with anti-MAYP antibodies showed that this was caused by contamination with blood monocytes (Figure 5G-H). MAYP staining was not observed in CD3$^+$ or B220$^+$ lymphocytes (Figure 5G-H). Similar analysis of the granulocyte fraction showed MAYP staining of the Mac1$^+$ subfraction of granulocytes (Figure 5I), representing approximately 9.5% of the total number of granulocytes. These results indicate that MAYP expression is restricted to monocytes and Mac1^{hi}Gr1^{hi} monocyte precursors in the mouse and to monocytes and a small subfraction of granulocytes in humans.

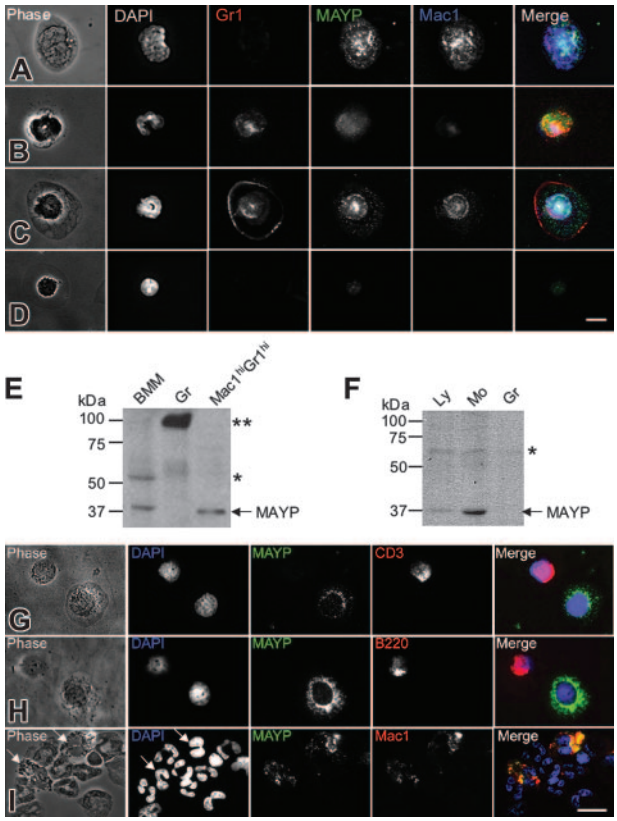

Figure 5. MAYP is expressed in macrophages and a subset of granulocytes in mice and humans. (A-D) Immunofluorescence staining of mouse peripheral blood leukocytes FACS-sorted based on Mac1 and Gr1 and cytocentrifuged onto fibronectin-coated coverslips, fixed, permeabilized, and stained with DAPI and anti-MAYP antibody, showing the pattern of MAYP staining in Mac1^{hi}Gr1^{lo} monocytes (A), Mac1^{lo}Gr1^{hi} granulocytes (B), Mac1^{hi}Gr1^{hi} monocytes or monocyte precursors (C), and Mac1^{lo}Gr1^{lo} lymphocytes (D). Note diffuse staining of MAYP in panel B and its exclusively nuclear staining in panel D compared with the punctate cytoplasmic staining characteristic of MAYP in panels A and C. Panels on the right represent merged signals of Mac-1 (blue), MAYP (green), and Gr1 (red). (E) SDS-PAGE and Western blot analysis of MAYP expression in mouse BMMs, granulocytes (Gr), and the Mac1^{hi}Gr1^{hi} fraction. (F) Western blot analysis of MAYP expression in lymphocyte (Ly; nonadherent peripheral blood mononuclear cells), monocyte (Mo; adherent peripheral blood mononuclear cells), and granulocyte (Gr) fractions of human peripheral blood. (E-F) Single and double asterisks indicate positions of cross-reactive protein bands. (G-I) Immunofluorescence staining of fractions from panel F. Ly fraction (G-H), showing contaminating MAYP$^+$ monocytes, and Gr fraction (I) showing MAYP staining of a Mac1$^+$ subfraction of the granulocytes (10% of total). Bars, 10 μm.

Requirement of macrophages for *Mayp*$^{Lp/Lp}$ lesion development

MAYP was selectively expressed in mouse macrophages[11] and macrophage precursors (Figure 5), and there was extensive infiltration of F4/80$^+$ macrophages into *Mayp*$^{Lp/Lp}$ lesions. To test whether macrophages were required for development of the inflammation, we depleted macrophages using clodronate liposomes.[28] Intraperitoneal administration of clodronate to 4-week-old *Mayp*$^{Lp/Lp}$ mice twice a week significantly depleted peripheral blood monocytes and peritoneal macrophages (data not shown) but had no effect on the inflammatory phenotype, possibly because of the failure of liposomes to efficiently exit the vascular compartment. However, simultaneous intraperitoneal and subcutaneous injections of the clodronate liposomes into the hind paws of mice once a week completely prevented the development of inflammation of the hind paws during the 4-week treatment period, whereas the same frequency, time of onset, and severity of inflammation of the forepaws were observed in control mice. In control mice injected with PBS liposomes, there was no change in frequency, onset, or severity of inflammation compared with untreated controls, and fore and hind paws were equally affected (Table 2 and data not shown). These results strongly implicate a role for the macrophages in the initial development of disease.

Reduced macrophage expression of MAYP in *Mayp*$^{Lp/Lp}$ mice

To determine the effect of the I282N mutation on MAYP expression, we examined MAYP levels in BMMs isolated from WT and *Mayp*$^{Lp/Lp}$ mice. SDS-PAGE and Western blotting revealed that the levels of MAYP in whole cell lysates of BMMs obtained from *Mayp*$^{Lp/Lp}$ mice were 0.34 ± 0.08 ($n = 3$) times the levels in BMMs from WT type mice (Figure 6A), and this was confirmed in Western blots of immunoprecipitated MAYP (Figure 6B). Quantitative RT-PCR analysis of the MAYP mRNA from BMMs revealed no significant difference in mRNA levels between *Mayp*$^{Lp/Lp}$ and WT BMMs (Figure 6C), suggesting that the *Lupo* mutation causes decreased expression of the mutant MAYP protein as a result of a reduced mRNA translation rate or reduced protein stability. Despite the lowered levels of MAYP, the tyrosine phosphorylation of MAYP in response to CSF-1 was preserved, though slightly delayed (data not shown). Because of the possible relevance of bacterial exposure to the development of the inflammatory lesions, we also examined the response of BMMs to LPS. Compared with WT BMMs, in which increases in the level of MAYP expression were significant at 24 hours, the increases in *Mayp*$^{Lp/Lp}$ BMMs were barely perceptible (Figure 6D). Indeed, in separate experiments, the increased MAYP expression in the *Mayp*$^{Lp/Lp}$ BMMs never attained the levels observed in unstimulated WT BMMs (0.68 ± 0.04 [$n = 3$] times levels in unstimulated WT mice). Thus, apart from possible qualitative effects of the I282N mutation, it is clear that the mutation leads to significant reductions in the steady state expression of

Table 2. Prevention of hind paw inflammation by combined intravenous and subcutaneous administration of clodronate liposomes

Characteristic	Control	Clodronate	
		Intraperitoneal injection only*	Intraperitoneal and subcutaneous injection*
Paws, no.	32	48	12
Median onset, d, 95% CIs	42 ± 8	40 ± 6	ND
Affected at 8 wk†, %	66	66	0§
Severe inflammation‡, %	43	40	0‖

ND indicates no disease.

*Injection intraperitoneally twice and subcutaneously once weekly for 4 weeks. Controls were injected intraperitoneally or subcutaneously, or both, with PBS liposomes.

†End of observation period.

‡Grade 3 or 4 (grades: 0, no inflammation; 1, slight restricted redness; 2, redness and swelling; 3, redness and massive swelling or affecting large areas; 4, redness and massive swelling or affecting large areas plus extended oozing or necrosis).

§$P < .001$; Kaplan-Meier analysis with post hoc log rank test.

‖$P < .01$; χ^2 analysis and Fisher exact test.

MAYP and the level of MAYP attained in response to LPS. To determine whether the induction of MAYP expression by LPS precedes or follows the elevation of proinflammatory cytokines, we stimulated WT BMMs with LPS for different times and measured the expression of MAYP, IL-1β, and TNF-α (Figure 6E). MAYP induction was substantially delayed compared with the elevation of the proinflammatory cytokines.

Elevated circulating cytokine level in *Mayp*$^{Lp/Lp}$ mice and altered cytokine response of Mayp$^{Lp/Lp}$ macrophages to LPS in vitro

Preliminary data revealed that compared with WT mice, *Mayp*$^{Lp/Lp}$ mice had elevated levels of IL-4, RANTES, TGF-β, and MCP-1, whereas no significant changes were observed for IL-2, IFN-γ, collagen VI, leptin, or TNF-α (data not shown). To investigate the alterations in macrophage cytokine production, the secretion of 40 cytokines by cultured WT and *Mayp*$^{Lp/Lp}$ BMM was determined, using a mouse inflammation antibody array. *Mayp*$^{Lp/Lp}$ BMMs cultured in the absence of LPS produced significantly more monocyte chemoattractant protein-1 (MCP-1) and soluble TNF receptor I (sTNFRI) than WT BMMs (Figure 7B). *Mayp*$^{Lp/Lp}$ BMMs cultured in the presence of LPS produced significantly less IFN-inducible T-cell α chemoattractant (I-TAC), stromal cell–derived factor-1 (SDF-1), T cell activation-3 (TCA-3), and tissue inhibitor of metalloproteinases-1 (TIMP-1) than WT BMMs (Figure 7C). No significant differences were observed for the other cytokines in these arrays.

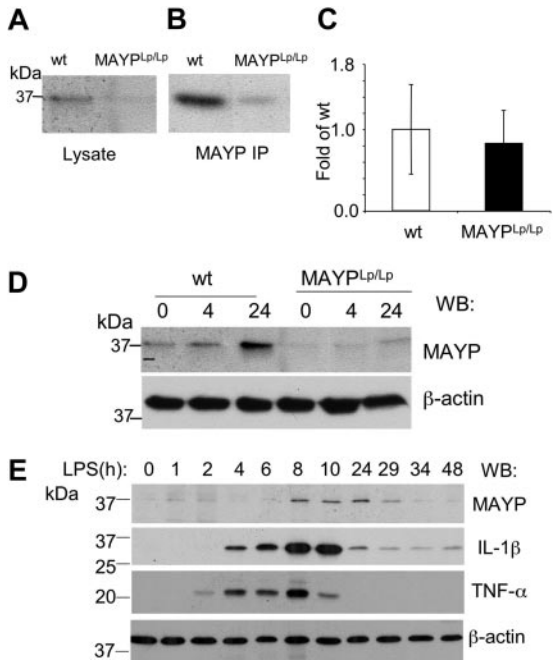

Figure 6. Reduced MAYP expression in *Mayp*$^{Lp/Lp}$ macrophages. SDS-PAGE and Western blot analysis of MAYP expression in NP-40 cell lysates (A) and anti-MAYP immunoprecipitates (B) prepared from BMMs of *Mayp*$^{Lp/Lp}$ and WT mice. (C) Similar levels of expression of MAYP mRNA in BMMs of *Mayp*$^{Lp/Lp}$ and WT mice determined by quantitative RT-PCR (± SD, triplicate assays, 2 mice per genotype). (D) LPS stimulation for 4 or 24 hours fails to elevate MAYP expression in *Mayp*$^{Lp/Lp}$ BMMs above the level of its expression in unstimulated WT BMMs. (E) Peak response of MAYP expression to LPS follows peak responses of the proinflammatory cytokines IL-1β and TNF-α. β-Actin is the loading control.

Discussion

By screening the homozygous progeny of mice bearing genome-wide mutations, we uncovered a recessive mouse mutation that confers a chronic inflammation phenotype involving the paws and skin. Positional cloning and DNA sequencing mapped this mutation, *Lupo (Lp)*, to a single-base substitution in the coding region of the Mayp/Pstpip2 locus on chromosome 18 that leads to the amino acid substitution I282N. Homozygous mutant *(Mayp*$^{Lp/Lp}$*)* mice exhibited a disease with all the hallmarks of an autoinflammatory disease. Bone marrow transplantation experiments demonstrated that the disease was of bone marrow origin. Despite high levels of circulating autoantibodies in mice with advanced disease, the disease developed more rapidly and with greater penetrance on a lymphocyte-deficient *Rag1*$^{-/-}$ background than on the *Rag1*$^{+/+}$ background, demonstrating that it developed independently of lymphocytes and that, far from enhancing disease development, lymphocytes have an ameliorating effect. Thus, autoantibody production appears to be secondary to macrophage-mediated tissue damage. Consistent with a macrophage-mediated disease, a prominent histologic feature of the early lesions is extensive infiltration of macrophages with few granulocytes. In a survey of mouse and human blood cells, MAYP was shown to be most prominently expressed in monocytes and monocyte precursors in mouse and in a small Mac1$^+$ subfraction of human granulocytes, which could also be macrophage progenitor cells.[29,30] Furthermore, clodronate treatment of *Mayp*$^{Lp/Lp}$ mice that selectively depletes macrophages from lesions completely inhibited the development of disease. Analysis of MAYP expression in *Mayp*$^{Lp/Lp}$ macrophages revealed that, despite normal expression of MAYP mRNA, MAYP protein was expressed at one third its level in WT macrophages, indicating that the mutation most likely affects posttranslational

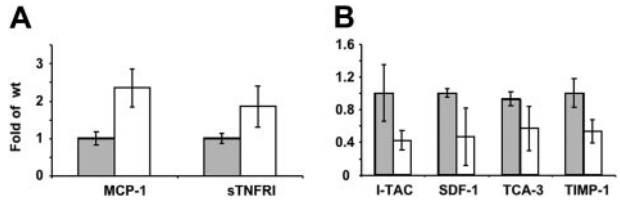

Figure 7. Differences in cytokine production by WT and *Mayp*$^{Lp/Lp}$ macrophages. (A) Cytokine release by cultured WT (▨) and *Mayp*$^{Lp/Lp}$ (□) BMM. (B) Cytokine release in WT (▨) and *Mayp*$^{Lp/Lp}$ (□) BMMs stimulated with LPS for 24 hours. Duplicate measurements for BMMs from 2 mice of each genotype. Differences between WT and *Mayp*$^{Lp/Lp}$ are significant ($P < .05$; Student t test; n = 4). No significant differences were seen for the other 34 cytokines tested and listed in "Materials and methods."

stability or mRNA translation. The effects of the I282N mutation on protein expression are particularly significant when one considers that stimulation of *Mayp*$^{Lp/Lp}$ macrophages with LPS, which normally induces a 3-fold increase in MAYP expression, failed to increase the level of expression enough to attain the level found in unstimulated WT macrophages. Interestingly, the LPS-induced elevation of MAYP followed the rapid induction of the proinflammatory cytokines TNF-α and IL-1β, consistent with the possibility that the MAYP response to LPS is part of a negative feedback loop. These studies point to an anti-inflammatory role for MAYP in the macrophage.

The most prevalent of the periodic fever syndromes, FMF, results from mutations in the gene encoding pyrin, a member of the death fold superfamily.[31,32] Pyrin has an N-terminal pyrin domain (PYD) homologous to the death domain, death effector domain, and caspase recruitment domain (CARD) subfamilies, all of which participate in homotypic protein–protein interactions and occur in proteins involved in apoptosis and inflammation.[33,34] Although pyrin has an important role in NF-κB transcription factor activation and apoptosis, its action is unclear.[4] Pyrin-deficient mice have a defect in macrophage apoptosis, and in vitro full-length pyrin competes with caspase-1 for binding to a known caspase-1 activator, ASC (apoptosis-associated speck-like protein containing a CARD) adaptor protein, thereby inhibiting the processing of pro–IL-1β to active IL-1β.[35]

It has recently been shown that the PAPA syndrome, characterized by polymorphonuclear leukocyte invasion of joints and skin, is caused by mutations in the PCH family member PSTPIP1, also known as CD2BP1.[6] PSTPIP1 is a tyrosine-phosphorylated cytoskeletal protein that binds to and is a substrate of protein tyrosine phosphatase PEST, localizing the enzyme for the specific dephosphorylation of Wiskott-Aldrich syndrome protein (WASP).[5,7,36] An important connection between pyrin and PSTPIP1, with respect to their involvement in a pathway common to FMF and PAPA syndromes, was recently made by the demonstration that pyrin interacts and colocalizes with PSTPIP1.[8] This interaction requires the phosphorylation of Y344 of PSTPIP1. Mutations in PSTPIP1 associated with PAPA syndrome (A230T and E250Q) reside in the PTP–PEST binding site of PSTPIP1, inhibiting PTP–PEST/PSTPIP1 interaction and consequently PSTPIP1 dephosphorylation at Y344 and leading to PSTPIP1 hyperphosphorylation and a marked increase in the association of PSTPIP1 with pyrin.[8] Consistent with the hypothesis that the increased association of PAPA mutant PSTPIP1s with pyrin inhibits the negative regulation of pro–IL-1β processing by pyrin, increased levels of IL-1β and downstream cytokine production were observed in peripheral white blood cells from a patient with PAPA.[8]

Our data clearly show that MAYP, like PSTPIP1, normally inhibits the development of autoinflammatory disease. However, the histologic data and the pattern of cytokine production suggest that they act through different mechanisms. First, in contrast to PAPA syndrome, which primarily involves neutrophil invasion[6,37] without reported lymphocyte involvement, the macrophage invasion in MAYP lesions predominates. Indeed, it may be the specialized antigen-processing role of the macrophage leading to the autoantibodies observed in *Mayp*$^{Lp/Lp}$ disease that have not been reported for PAPA syndrome. Second, our cytokine experiments indicate that there is no significant increase in LPS-stimulated secretion of IL-1β or TNF-α in *Mayp*$^{Lp/Lp}$ macrophages, in contrast to the LPS-induced elevation of IL-1β in PAPA syndrome leukocytes[8] and the successful treatment of pyoderma gangrenosum with inhibitors of TNF-α.[38,39] However, we found elevated levels of MCP-1 and sTNFRI, which could have contributed to disease. MCP-1 is chemotactic for monocytes, but not neutrophils, and its production by macrophages within lesions might have increased monocyte recruitment.[40] Furthermore, MCP-1 is osteoclastogenic,[41] and increased numbers of osteoclasts could be responsible for the osteolysis. Increased sTNFRI could contribute to inflammation by scavenging for TNF and reducing macrophage apoptosis. In an NC/Nga mouse model of atopic dermatitis, disease is reduced when toenails are clipped[42] and fails to develop in specific pathogen-free conditions.[43] Thus, the location of lesions in the paws and ears of *Mayp*$^{Lp/Lp}$ mice is probably due to cutaneous infections that occur as a result of normal grooming behavior. Relevant to bacterial exposure in the development of the inflammatory lesions, stimulation with LPS revealed decreased production of I-TAC, SDF-1, TCA-3, and TIMP-1 by *Mayp*$^{Lp/Lp}$ macrophages. It is conceivable that the reduced production of I-TAC, which is a potent chemoattractant for activated T_H1 and NK cells,[44] and TCA-3, which is a chemoattractant for T_H2 cells,[45] decreases the infiltration of regulatory T and NK cells to the lesion, consistent with the increased severity of *Mayp*$^{Lp/Lp}$ disease on the *Rag1*$^{-/-}$ background. Reduction in the TIMP-1 level may allow stronger matrix metalloproteinase–mediated tissue damage, which could enhance the production of autoantibodies.[46]

At present, no known diseases have been reported to be associated with the genes encoding MAYP in humans. However, mutations in regions of the human genome (18q12-18q22) syntenic with the region encoding mouse *Mayp/Pstpip2* (chromosome 18 E3) have been associated with multiple autoimmune or autoinflammatory diseases, including type 1 diabetes, multiple sclerosis, rheumatoid arthritis, juvenile idiopathic arthritis, and chronic recurrent multifocal osteomyelitis.[47-49] Recently, a mutation in the chronic multifocal osteomyelitis *(cmo)* mouse[50] was associated with an L98P amino acid substitution in MAYP.[51] Although it was not formally established that this mutation was responsible for the *cmo* phenotype and though the disease has not been characterized in detail, these findings suggest that another mutation in the *Mayp* gene can result in a disease similar to the disease exhibited by *Mayp*$^{Lp/Lp}$ mice. In our study, the probability that an unidentified passenger mutation physically linked to *Mayp*^{Lp} was responsible for the autoinflammatory disease phenotype was determined to be 0.000016; we concluded, therefore, that the *Mayp*^{Lp} mutation causes the phenotype.

The present studies demonstrate that low levels of MAYP are associated with abnormal macrophage activation, resulting in tissue necrosis and bone destruction. Our previous work demonstrated that lowering MAYP expression in a macrophage cell line to approximately 30% resulted in a discernible morphologic phenotype and decreased CSF-1–mediated chemotaxis.[15] Given that in preliminary experiments we were unable to observe a similar phenotype in *Mayp*$^{Lp/Lp}$ macrophages (V.C., unpublished observations, March 2005), it will be of interest to determine whether other effects of the I282N mutation, in addition to decreased MAYP expression, contribute to this disease.

Acknowledgments

We thank Xiao-Hua Zong and Ranu Basu for technical assistance and members of the Albert Einstein College of Medicine histopathology facility for assistance with different aspects of this work. We thank Dr D. A. Hume for the F4/80 antibody.

References

1. Galon J, Aksentijevich I, McDermott MF, O'Shea JJ, Kastner DL. TNFRSF1A mutations and autoinflammatory syndromes. Curr Opin Immunol. 2000;12:479-486.
2. McDermott MF, Aksentijevich I, Galon J, et al. Germline mutations in the extracellular domains of the 55 kDa TNF receptor, TNFR1, define a family of dominantly inherited autoinflammatory syndromes. Cell. 1999;97:133-144.
3. Hull KM, Drewe E, Aksentijevich I, et al. The TNF receptor-associated periodic syndrome (TRAPS): emerging concepts of an autoinflammatory disorder. Medicine (Baltimore). 2002;81:349-368.
4. McDermott MF. A common pathway in periodic fever syndromes. Trends Immunol. 2004;25:457-460.
5. Spencer S, Dowbenko D, Cheng J, et al. PSTPIP: a tyrosine phosphorylated cleavage furrow-associated protein that is a substrate for a PEST tyrosine phosphatase. J Cell Biol. 1997;138:845-860.
6. Wise CA, Gillum JD, Seidman CE, et al. Mutations in CD2BP1 disrupt binding to PTP PEST and are responsible for PAPA syndrome, an autoinflammatory disorder. Hum Mol Genet. 2002;11:961-969.
7. Dowbenko D, Spencer S, Quan C, Lasky L. Identification of a novel polyproline recognition site in the cytoskeletal associated protein, proline serine threonine phosphatase interacting protein. J Biol Chem. 1998;273:989-996.
8. Shoham NG, Centola M, Mansfield E, et al. Pyrin binds the PSTPIP1/CD2BP1 protein, defining familial Mediterranean fever and PAPA syndrome as disorders in the same pathway. Proc Natl Acad Sci U S A. 2003;100:13501-13506.
9. Lippincott J, Li R. Involvement of PCH family proteins in cytokinesis and actin distribution. Microsc Res Tech. 2000;49:168-172.
10. Wu Y, Spencer SD, Lasky LA. Tyrosine phosphorylation regulates the SH3-mediated binding of the Wiskott-Aldrich syndrome protein to PSTPIP, a cytoskeletal-associated protein. J Biol Chem. 1998;273:5765-5770.
11. Yeung YG, Soldera S, Stanley ER. A novel macrophage actin-associated protein (MAYP) is tyrosine-phosphorylated following colony stimulating factor-1 stimulation. J Biol Chem. 1998;273:30638-30642.
12. Wu Y, Dowbenko D, Lasky LK. PSTPIP 2, a second tyrosine phosphorylated, cytoskeletal associated protein that binds a PEST-type protein-tyrosine phosphatase. J Biol Chem. 1998;273:30487-30496.
13. Ho HY, Rohatgi R, Lebensohn AM, et al. Toca-1 mediates Cdc42-dependent actin nucleation by activating the N-WASP-WIP complex. Cell. 2004;118:203-216.
14. Tian L, Nelson DL, Stewart DM. Cdc42-interacting protein 4 mediates binding of the Wiskott-Aldrich syndrome protein to microtubules. J Biol Chem. 2000;275:7854-7861.
15. Chitu V, Pixley FJ, Macaluso F, et al. The PCH family member MAYP/PSTPIP2 directly regulates F-actin bundling and enhances filopodia formation and motility in macrophages. Mol Biol Cell. 2005;16:2947-2959.
16. Pixley FJ, Stanley ER. CSF-1 regulation of the wandering macrophage: complexity in action. Trends Cell Biol. 2004;14:628-638.
17. Nicklas W, Baneux P, Boot R, et al. Recommendations for the health monitoring of rodent and rabbit colonies in breeding and experimental units. Lab Anim. 2002;36:20-42.
18. Augustin M. Efficient and fast targeted production of murine models based on chemical mutagenesis. Mamm Genome. 2005;16:405-413.
19. Yu P, Constien R, Dear N, et al. Autoimmunity and inflammation due to a gain-of-function mutation in phospholipase C gamma 2 that specifically increases external Ca2+ entry. Immunity. 2005;22:451-465.
20. Van Rooijen N, Sanders A. Liposome mediated depletion of macrophages: mechanism of action, preparation of liposomes and applications. J Immunol Methods. 1994;174:83-93.
21. Dai XM, Ryan GR, Hapel AJ, et al. Targeted disruption of the mouse colony-stimulating factor 1 receptor gene results in osteopetrosis, mononuclear phagocyte deficiency, increased primitive progenitor cell frequencies, and reproductive defects. Blood. 2002;99:111-120.
22. Boyum A. Isolation of lymphocytes, granulocytes and macrophages. Scand J Immunol. 1976;(suppl 5):9-15.
23. Stanley ER. Murine bone marrow-derived macrophages. In: Walker JM, Pollard JW, eds. Animal Cell Culture. 2nd ed. Totowa, NJ: Humana Press; 1997:301-304.
24. Tushinski RJ, Oliver IT, Guilbert LJ, Tynan PW, Warner JR, Stanley ER. Survival of mononuclear phagocytes depends on a lineage-specific growth factor that the differentiated cells selectively destroy. Cell. 1982;28:71-81.
25. Mombaerts P, Iacomini J, Johnson RS, Herrup K, Tonegawa S, Papaioannou VE. RAG-1-deficient mice have no mature B and T lymphocytes. Cell. 1992;68:869-877.
26. Guilbert LJ, Stanley ER. Specific interaction of murine colony-stimulating factor with mononuclear phagocytic cells. J Cell Biol. 1980;85:153-159.
27. Biermann H, Pietz B, Dreier R, Schmid KW, Sorg C, Sunderkötter C. Murine leukocytes with ring-shaped nuclei include granulocytes, monocytes, and their precursors. J Leuk Biol. 1999;65:217-231.
28. van Rooijen N, van Kesteren-Hendrikx E. Clodronate liposomes: perspectives in research and therapeutics. J Liposome Res. 2002;12:81-94.
29. Buhles WC Jr. Studies on mononuclear phagocyte progenitor cells: morphology of cells and colonies in liquid culture of mouse bone marrow. J Reticuloendothel Soc. 1979;25:363-378.
30. Pels E, De Groot JW, Mullink R, Van Unnik JA, den Otter W. Identification of two different types of mouse peritoneal exudate cells with ring-shaped nuclei. J Reticuloendothel Soc. 1980;27:367-376.
31. Bertin J, DiStefano PS. The PYRIN domain: a novel motif found in apoptosis and inflammation proteins. Cell Death Differ. 2000;7:1273-1274.
32. Martinon F, Hofmann K, Tschopp J. The pyrin domain: a possible member of the death domain-fold family implicated in apoptosis and inflammation. Curr Biol. 2001;11:R118-R120.
33. Wang L, Manji GA, Grenier JM, et al. PYPAF7, a novel PYRIN-containing Apaf1-like protein that regulates activation of NF-kappa B and caspase-1-dependent cytokine processing. J Biol Chem. 2002;277:29874-29880.
34. Manji GA, Wang L, Geddes BJ, et al. PYPAF1, a PYRIN-containing Apaf1-like protein that assembles with ASC and regulates activation of NF-kappa B. J Biol Chem. 2002;277:11570-11575.
35. Chae JJ, Komarow HD, Cheng J, et al. Targeted disruption of pyrin, the FMF protein, causes heightened sensitivity to endotoxin and a defect in macrophage apoptosis. Mol Cell. 2003;11:591-604.
36. Côté JF, Charest A, Wagner J, Tremblay ML. Combination of gene targeting and substrate trapping to identify substrates of protein tyrosine phosphatases using PTP-PEST as a model. Biochemistry. 1998;37:13128-13137.
37. Callen JP. Neutrophilic dermatoses. Dermatol Clin. 2002;20:409-419.
38. Cortis E, De Benedetti F, Insalaco A, et al. Abnormal production of tumor necrosis factor (TNF) alpha and clinical efficacy of the TNF inhibitor etanercept in a patient with PAPA syndrome [published correction appears in J Pediatr. 2005;146:193]. J Pediatr. 2004;145:851-855.
39. Stichweh DS, Punaro M, Pascual V. Dramatic improvement of pyoderma gangrenosum with infliximab in a patient with PAPA syndrome. Pediatr Dermatol. 2005;22:262-265.
40. Yoshimura T, Leonard EJ. Human monocyte chemoattractant protein-1: structure and function. Cytokines. 1992;4:131-152.
41. Kim MS, Day CJ, Morrison NA. MCP-1 is induced by receptor activator of nuclear factor-κB ligand, promotes human osteoclast fusion, and rescues granulocyte macrophage colony-stimulating factor suppression of osteoclast formation. J Biol Chem. 2005;280:16163-16169.
42. Hashimoto Y, Arai I, Nakanishi Y, Sakurai T, Nakamura A, Nakaike S. Scratching of their skin by NC/Nga mice leads to development of dermatitis. Life Sci. 2004;76:783-794.
43. Matsuda H, Watanabe N, Geba GP, et al. Development of atopic dermatitis-like skin lesion with IgE hyperproduction in NC/Nga mice. Int Immunol. 1997;9:461-466.
44. Cole KE, Strick CA, Paradis TJ, et al. Interferon-inducible T cell alpha chemoattractant (I-TAC): a novel non-ELR CXC chemokine with potent activity on activated T cells through selective high affinity binding to CXCR3. J Exp Med. 1998;187:2009-2021.
45. Goya I, Gutierrez J, Varona R, Kremer L, Zaballos A, Marquez G. Identification of CCR8 as the specific receptor for the human beta-chemokine I-309: cloning and molecular characterization of murine CCR8 as the receptor for TCA-3. J Immunol. 1998;160:1975-1981.
46. Descamps FJ, Van den Steen PE, Nelissen I, Van Damme J, Opdenakker G. Remnant epitopes generate autoimmunity: from rheumatoid arthritis and multiple sclerosis to diabetes. Adv Exp Med Biol. 2003;535:69-77.
47. Merriman TR, Cordell HJ, Eaves IA, et al. Suggestive evidence for association of human chromosome 18q12-q21 and its orthologue on rat and mouse chromosome 18 with several autoimmune diseases. Diabetes. 2001;50:184-194.
48. Golla A, Jansson A, Ramser J, et al. Chronic recurrent multifocal osteomyelitis (CRMO): evidence for a susceptibility gene located on chromosome 18q21.3-18q22. Eur J Hum Genet. 2002;10:217-221.
49. Rosen P, Hopkin RJ, Glass DN, Graham TB. Another patient with chromosome 18 deletion syndrome and juvenile rheumatoid arthritis. J Rheumatol. 2004;31:998-1000.
50. Byrd L, Grossmann M, Potter M, Shen-Ong GL. Chronic multifocal osteomyelitis, a new recessive mutation on chromosome 18 of the mouse. Genomics. 1991;11:794-798.
51. Ferguson PJ, Bing X, Vasef MA, et al. A missense mutation in pstpip2 is associated with the murine autoinflammatory disorder chronic multifocal osteomyelitis. Bone. 2006;38:41-47.